What Can We Learn about the Unstable Equation-of-state Branch from Neutron Star Mergers?

Maximiliano Ujevic[1] , Rahul Somasundaram[2,3] , Tim Dietrich[4,5] , Jerome Margueron[6,7], and Ingo Tews[2]
[1] Centro de Ciências Naturais e Humanas, Universidade Federal do ABC, Santo André, 09210-170, SP, Brazil
[2] Theoretical Division, Los Alamos National Laboratory, Los Alamos, NM 87545, USA
[3] Department of Physics, Syracuse University, Syracuse, NY 13244, USA
[4] Institute for Physics and Astronomy, University of Potsdam, D-14476 Potsdam, Germany
[5] Max Planck Institute for Gravitational Physics (Albert Einstein Institute), Am Mühlenberg 1, Potsdam 14476, Germany
[6] Institut de Physique des 2 infinis de Lyon, CNRS/IN2P3, Université de Lyon, Université Claude Bernard Lyon 1, F-69622 Villeurbanne Cedex, France
[7] International Research Laboratory on Nuclear Physics and Astrophysics, Michigan State University and CNRS, East Lansing, MI 48824, USA

Abstract

The equation of state (EOS) of dense strongly interacting matter can be probed by astrophysical observations of neutron stars (NS), such as X-ray detections of pulsars or the measurement of the tidal deformability of NSs during the inspiral stage of NS mergers. These observations constrain the EOS at most up to the density of the maximum-mass configuration, $n_{\rm TOV}$, which is the highest density that can be explored by stable NSs for a given EOS. However, under the right circumstances, binary neutron star (BNS) mergers can create a postmerger remnant that explores densities above $n_{\rm TOV}$. In this work, we explore whether the EOS above $n_{\rm TOV}$ can be measured from gravitational-wave or electromagnetic observations of the postmerger remnant. We perform a total of 25 numerical-relativity simulations of BNS mergers for a range of EOSs and find no case in which different descriptions of the matter above $n_{\rm TOV}$ have a detectable impact on postmerger observables. Hence, we conclude that the EOS above $n_{\rm TOV}$ can likely not be probed through BNS merger observations for the current and next generation of detectors.

1. Introduction

The equation of state (EOS) of dense matter is a fundamental relation in nuclear (astro)physics. It connects the properties of strong interactions among the relevant microscopic degrees of freedom, described by quantum chromodynamics (QCD), to the global properties of neutron stars (NSs), such as their masses, radii, and tidal deformabilities. In recent years, astrophysical measurements of NS properties from X-ray (Miller & others NICER collaboration 2019; Riley & others NICER collaboration 2019; Miller & others NICER collaboration 2021; Riley & others NICER collaboration 2021), radio (Demorest et al. 2010; Antoniadis et al. 2013; Cromartie et al. 2019; Fonseca et al. 2021), and gravitational-wave (GW) observations of the inspiral phase of binary neutron star (BNS) mergers (Abbott et al. 2017, 2018, 2019, 2020) have provided a wealth of information on the EOS (see, e.g., Bauswein et al. 2017; Margalit & Metzger 2017; Annala et al. 2018; Most et al. 2018; Ruiz et al. 2018; Landry & Essick 2019; Radice & Dai 2019; Capano et al. 2020; Dietrich et al. 2020; Essick et al. 2020; Raaijmakers et al. 2020, 2021; Ghosh et al. 2022; Huth et al. 2022; Pang et al. 2022). While these observations already led to exciting results, the era of high-precision astrophysical measurements of the EOS is yet to come, with the next generation of GW detectors being planned in the United States (Reitze et al. 2019; Evans & others Cosmic Explorer Consortium 2021) and Europe (Punturo et al. 2010; Branchesi et al. 2023), and improved large-area X-ray timing telescopes

anticipated in the future (e.g., Gaskin et al. 2019; Mushotzky et al. 2019; Zhang et al. 2019).

The EOS of dense matter links the pressure p, energy density ϵ, and the number density n, spanning from very dilute matter up to asymptotically large densities where the dynamics of QCD become perturbative, $n \sim 40 n_{\rm sat}$, with $n_{\rm sat}$ being the nuclear saturation density. However, stable NSs probe the EOS only up to the central density of the maximum-mass configuration, which we call the TOV density $n_{\rm TOV}$ in the following. This limit results from the general relativity (GR) structure equations for NSs, the Tolman-Oppenheimer-Volkoff (TOV) equations, and depends on the EOS for $n \leqslant n_{\rm TOV}$. While the exact value of $n_{\rm TOV}$ is unknown, present astrophysical observations place it at $n_{\rm TOV} \sim 5$–$8 n_{\rm sat}$ (Pang et al. 2022).

Consequently, observations of pulsars or NS inspirals cannot probe the EOS above $n_{\rm TOV}$. Nevertheless, the EOS above $n_{\rm TOV}$ is of great interest. Its properties might affect $n_{\rm TOV}$ because it is possible that a strong softening, such as a phase transition slightly above $n_{\rm TOV}$, destabilizes NSs and hence, setting the properties of the maximum-mass configuration to begin with. Furthermore, in the postmerger phase of BNS collisions, despite the fact that the rapidly rotating remnant typically reaches densities lower than in the nonrotating case, e.g., Figure 3 in Camelio et al. (2021), the EOS above $n_{\rm TOV}$ might still be relevant to describe postmerger physics, such as the postmerger GW signal or the mass of the ejecta and hence, the kilonova lightcurves.

Additionally, there can be cases where the appearance of new degrees of freedom may change the maximum mass of the EOS and so $n_{\rm TOV}$. Therefore, by comparing the outcomes and stability of two almost identical EOSs, it would be possible to
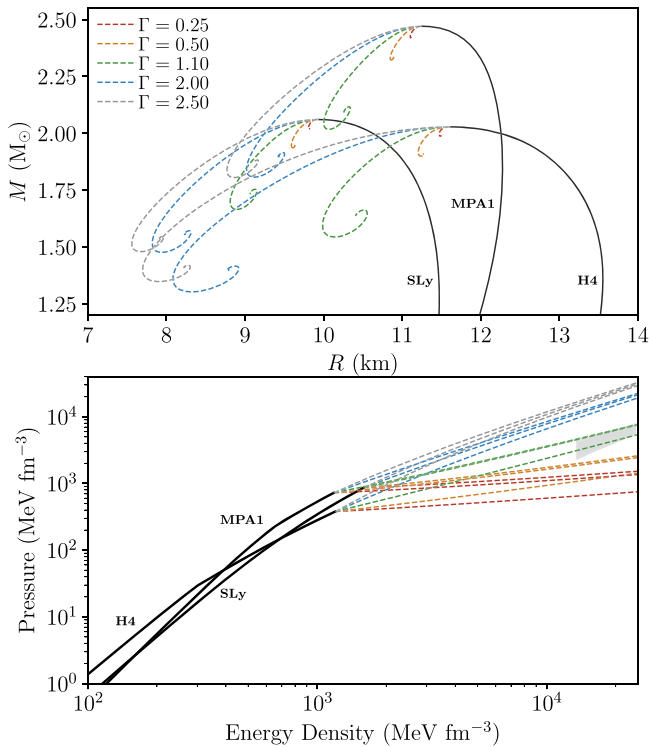
Figure 1. Upper panel: mass–radius curves for the three stable-branch EoSs employed in this work. The EoSs have different compactness and maximum masses, covering a considerable portion of the NS parameter space. With dashed lines and different colors, we represent the various extensions for the unstable branches. Bottom panel: pressure vs. energy density for the EoSs and extensions used in this work. The gray area shows the perturbative QCD domain.

learn something beyond the maximum density of at least one of the two EOSs.

In this Letter, we systematically investigate the possibility of measuring the EOS above n_{TOV} with observations of the postmerger remnant of BNS mergers. We perform a simulation campaign with 15 EOSs, considering different behavior for the stable and unstable branches; see Figure 1. We examine the GWs emitted by the remnant, the maximum density explored in the simulation, and the ejecta masses in detail and find that, in all considered cases, there is no detectable impact of the EOS above n_{TOV} on any observable related to the postmerger phase. Our findings establish n_{TOV} as a firm limit up to which physicists can hope to probe the EOS with astrophysical data. They further indicate that, given the expected uncertainties in the next decades, accurate knowledge of the cold and hot EOSs below n_{TOV} is sufficient for the prediction of postmerger observables such as the ejecta mass and the GW waveform.

2. Setup

2.1. Equations of State

In this study, we perform a simulation campaign with 15 different EOSs. These EOSs explore different behavior in the stable and unstable NS branches. In particular, we employ the SLy (Douchin & Haensel 2001), MPA1 (Müther et al. 1987), and H4 (Lackey et al. 2006) EOSs up to n_{TOV}. These EOSs are implemented in the form of their polytropic approximations from Read et al. (2009). All three EOSs explore different NS radii, ranging from $\sim$11.5–13.5 km for a typical $1.4\,M_{\mathrm{sol}}$ NS. The SLy and H4 EOS have similar maximum masses of

$\sim$2 M_{sol}, while the MPA1 EOS has a maximum mass of $\sim$2.5 M_{sol}. Hence, these three EOSs represent different possible behaviors in the stable NS branch (see Figure 1) and enable us to test the impact of this part of the EOS.

To probe the impact of the unstable branch, we attach another polytropic segment at n_{TOV} to each EOS. For this segment, we vary the polytropic index Γ between 0.25 and 2.5, exploring different stiffness in the unstable branch up to high densities (see Figure 1). At the highest densities, $n \sim 40 n_{\mathrm{sat}}$, the EOS can be constrained by perturbative QCD (pQCD) calculations (Gorda et al. 2018, 2021, 2023b). Our EOSs with $\Gamma = 1.1$ are consistent with results from pQCD in the p–ϵ plane, while the other extensions are either too soft or too stiff to be in agreement with pQCD.

Komoltsev & Kurkela (2022) showed that pQCD calculations can also constrain the EOS at lower densities by imposing causality and thermodynamic consistency of the EOS with high-density pQCD calculations. Using this approach, Gorda et al. (2023a) outlined that pQCD impacts the EoS of stable NSs while Somasundaram et al. (2023) found that the integral pQCD constraints have a marginal impact on the NS EoS selection once nuclear physics and astrophysical sources of information are accounted for. However, pQCD impacts the EOS in the unstable branch above n_{TOV} (see Figure 1). The present work will allow us to quantify more generally if densities above n_{TOV} can be measured through astrophysical observations.

### 2.2. Numerical Relativity Simulations

For the construction of our initial configurations, we are using the pseudo-spectral SGRID code (Tichy 2009, 2012; Dietrich et al. 2015b; Tichy et al. 2019). SGRID uses surface fitting coordinates to solve the Einstein equations following the extended conformal thin sandwich formulation (York 1999).

For the dynamical simulations, we use the finite-differencing numerical-relativity (NR) code BAM (Bruegmann et al. 2008; Thierfelder et al. 2011a; Dietrich et al. 2015a; Bernuzzi & Dietrich 2016; Dietrich et al. 2018). We use the Z4c formulation for the spacetime evolution (Bernuzzi & Hilditch 2010; Hilditch et al. 2013), the moving puncture gauge (Bona et al. 1996; Alcubierre et al. 2003; van Meter et al. 2006), and the Valencia formulation for general-relativistic hydrodynamics (Marti et al. 1991; Banyuls et al. 1997; Anton et al. 2006) together with high-resolution shock-capturing techniques for the description of matter variables. For the BAM simulations, we augment the cold EOSs described before with a Γ-law EOS using $\Gamma_{\mathrm{thermal}} = 1.75$ to incorporate thermal effects (Bauswein et al. 2010).

To ensure that we can resolve the relevant length scales, i.e., the far-field region in which GWs are extracted, but also the matter flow inside the stars, BAM uses a box-in-box mesh refinement that automatically can follow the movement of the stars. A Berger–Colella refinement strategy ensures stable and accurate simulations (Dietrich et al. 2015a). For this work, we employ a total of seven refinement levels and a resolution of approximately 108 m in the finest one.

3. Results

To quantify the possible impact of the EOS in the unstable branch above n_{TOV}, we will discuss the evolution of the maximum density and the black hole formation (Figure 2),
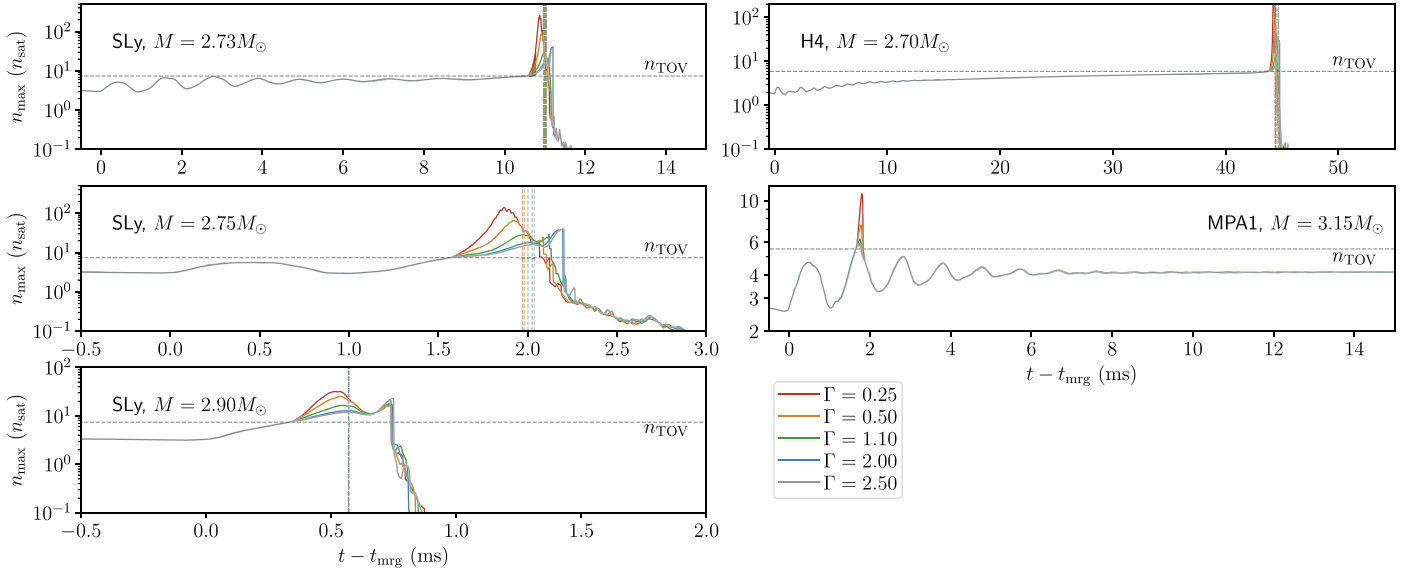
Figure 2. Time evolution of the maximum density, n_{max}, for all 25 simulations. We mark the maximum density present inside a nonrotating NS at the TOV mass (n_{TOV}) with a horizontal dashed line. In most cases, once this density is reached, the remnant collapses quickly into a black hole. However, our MPA1 $M = 3.15\,M_{\odot}$ is a clear exception where, for a short amount of time, the central density exceeds n_{TOV}, but the mass contained in the central region of the remnant is not large enough to trigger black hole formation. When available, we plot as vertical lines the time when the apparent horizon is first found in our simulation.
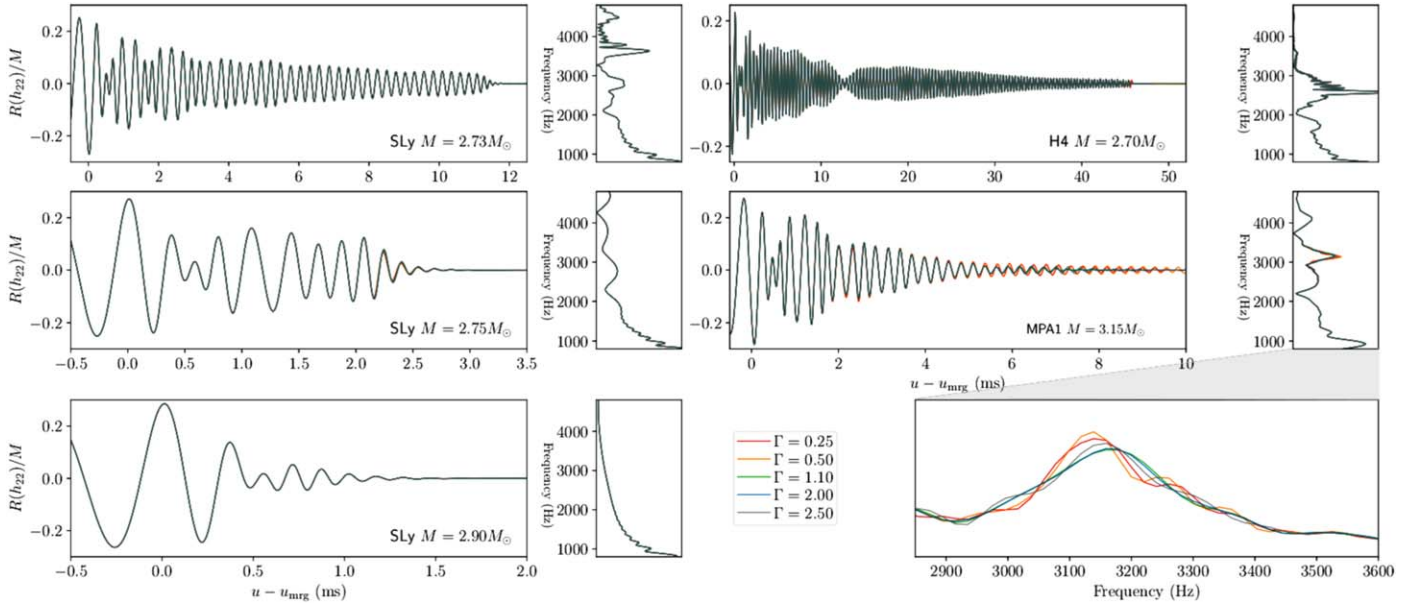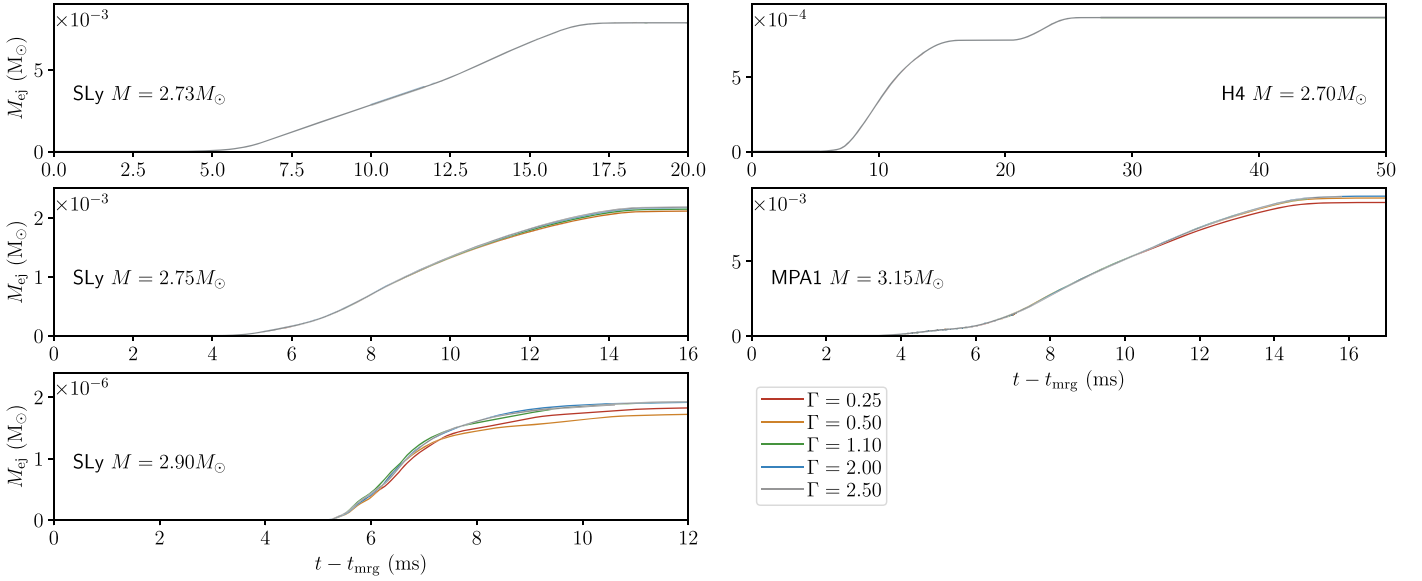

Figure 3. GW strain for all considered scenarios. We show the real part of the (2, 2) mode of the GW signal in the main panels and the corresponding spectrograms from the entire simulation in the smaller panels. We find a visible difference between the simulations with different high-density EOSs only for one scenario, the MPA1-like simulations, and present an inset of the spectrogram in the bottom right panel of the figure. While there is a shift in the peak frequency of about 30 Hz, the widths of the individual peaks are significantly larger. This will make it almost impossible to distinguish between the different EOSs, even with future-generation GW detectors.

outline possible impacts on the postmerger GW signal (Figure 3), and report on the released ejecta mass (Figure 4).

3.1. Density Evolution and Black Hole Formation

For our SLy-EOS simulations, we consider three different total masses: $2.73\,M_{\odot}$, $2.75\,M_{\odot}$, and $2.90\,M_{\odot}$ (left panels of Figure 2). Considering the $2.73\,M_{\odot}$ setup, we find a difference in the collapse time, i.e., the time between merger and formation of a black hole, of about $\mathcal{O}(100\mu s)$ for the different EOS extensions. This time difference is too small to be detectable in upcoming BNS merger observations. Overall, our

findings suggest that a black hole forms very quickly once the central density reaches n_{TOV}. Once this critical density is reached, higher densities are present during the ongoing simulation, and the evolution differs between the different setups. Surprisingly, we find that the densities peak before the formation of an apparent horizon, reported as vertical dashed lines in Figure 2. We note that there is a high chance that the apparent horizon formed earlier but was not tracked by the employed algorithm immediately, i.e., the dashed lines report an upper bound on the time when a black hole forms. We believe that, in practice, the highest densities are reached within a region either located inside the formed apparent horizon or in

Figure 4. The ejecta mass for all considered EOS scenarios as a function of time. The ejecta masses are extracted on a sphere with a coordinate radius of about 600 km.

a region where an apparent horizon forms very quickly. The densities drop once they reach the singularity since (i) the employed shift conditions excise the central singularity, and (ii) once the fluxes become infinite (or extremely large), the matter is removed from our grid (Thierfelder et al. 2011b). In general, we find that this drop in the density happens slightly later for larger values of Γ, likely due to the larger pressure for larger values of Γ.

For the $2.75\,M_\odot$ scenario, there is a small shift in the collapse time and a slight difference in the simulation once $n_{\rm TOV}$ is exceeded. However, the time difference is again $\mathcal{O}(100\mu s)$. Finally, for the $2.90\,M_\odot$ simulation, we find that the collapse to a black hole happens within 1 ms after the merger for all setups almost independently of the EOS extension, i.e., there is no measurable difference between the individual scenarios.

The previous simulations all use the same stable-branch EOS. To explore the impact of the stable branch, we also consider two other EOSs. For the H4 setup, we chose a total mass of $2.70\,M_\odot$ for our simulation to ensure that the merger remnant reaches densities above $n_{\rm TOV}$. In this case, the remnant survives for more than 40 ms before a black hole forms. We find that although the collapse happens much later than for the SLy scenarios, there is almost no difference between different values of Γ above $n_{\rm TOV}$.

Finally, we studied the MPA1 EOS with the highest maximum mass. For this setup, we carefully fine-tuned the masses performing different (low-resolution) simulations and settled on a total mass of $3.15\,M_\odot$, which shows overall the largest imprint of the unstable branch. For this setup, we did not observe a collapse to a black hole during the time of our simulation. However, we found that the star surpasses $n_{\rm TOV}$ about 2 ms after the merger but did not form a black hole (increasing the total mass led to black hole formation). On the contrary, the star's central density decreases again, continuing the density oscillation. This is of particular interest since it implies that for a short amount of time, higher densities than $n_{\rm TOV}$ were probed. Nevertheless, this effect does not lead to detectable differences.

These results are quite interesting. Long lifetimes lead to remnants that explore central densities well below $n_{\rm TOV}$, minimizing the impact of the unstable branch. When increasing the mass and reducing the lifetime of the remnant, appearing differences become undetectably short. From our investigations, we find that there seems to be no "sweet spot" where the unstable branch has a discernable impact.

3.2. Gravitational Waves

For the computation of the predicted GW signals, we are extracting the Newman–Penrose scalar Ψ_4 on an extraction sphere of radius about 1200 km around the origin of our computational domain and then compute the GW strain $h(t) = -\int_{-\infty}^{t}\int_{-\infty}^{t'}\Psi_4 dt''dt'$ following Reisswig & Pollney (2011). We show the GW strain and the corresponding power spectrum from the entire simulation in Figure 3. We find a perfect agreement for all SLy-like and H4-like simulations, i.e., no noticeable imprint of the unstable EOS branch on the GW signals is visible. Only for the MPA1 EOS do we find a slight difference in the GW signal due to a small shift in the oscillation of the remnant around 2 ms after the merger (see Figure 2). This difference results in a shift of about 30 Hz in the GW peak frequency between the most extreme scenarios, for $\Gamma = 0.25$ and $\Gamma = 2.50$. This value is lower than the numerical uncertainty of our simulation, which we estimate to be around 70 Hz by performing simulations with a grid spacing of about 130 m. Previous studies revealed measurement uncertainties of the peak frequency of about 50–100 Hz for close BNS mergers for which the postmerger signal-to-noise ratio (S/N) would be of the order $\mathcal{O}(10)$ (see, e.g., Clark et al. 2016; Rezzolla & Takami 2016; Breschi et al. 2022; or Branchesi et al. 2023). We also point out that it would be extremely difficult to have a shift due to the unstable-branch EOS from other effects, such as magnetic fields or neutrino radiation. For these reasons, we do not expect that similar differences would be detectable in the postmerger spectrum in future GW observations.

Overall, considering the need to fine-tune the system parameters to find imprints of the unstable EOS branch on the emitted GW signal and the minimal frequency shifts in the

postmerger peak frequency, we conclude that it is unlikely that GW information can be used to access the unstable EOS branch.

3.3. Ejecta

In addition to the emitted GW signals, observations of electromagnetic counterparts might help us to distinguish between different EOSs in the unstable branch. Given that the brightness of the electromagnetic counterparts is mainly proportional to the amount of ejected material, we will use the mass of ejected matter as an indicator for the possibility to differentiate between the different scenarios considered in this work. For this reason, we track outward-flowing, unbound material (using the geodesic criterion, i.e., $u_t < -1$). The extraction sphere is centered around the origin and has a radius of about 600 km.

For our SLy-like simulations, we generally find a decreasing ejecta mass with an increasing total mass. However, we do not find a measurable signal for different extensions of the EOS above $n_{\rm TOV}$. Similarly, also for the H4 and MPA1 setups, the differences in ejecta masses for the various EOS extensions are below $10^{-4} M_\odot$. This difference is well below the measurement uncertainties of current electromagnetic observations of a kilonova and its modeling uncertainties due to incomplete knowledge of opacities, heating rates, or thermal efficiencies (Dietrich et al. 2020; Heinzel et al. 2021; Fryer et al. 2023). Therefore, we can conclude that for all employed scenarios, we will not be able to access the EOS above $n_{\rm TOV}$ through the observations of electromagnetic counterparts.

4. Summary and Conclusions

Given previous studies about the possibility of measuring the high-density EOS from NS mergers, e.g., Most et al. (2019), Bauswein et al. (2019), and Figura et al. (2020), we have extended this question in this Letter and have investigated if binary NS mergers could provide us with meaningful information about the unstable branch of the EOS, i.e., the EOS at densities beyond the maximum density of a nonrotating single neutron star. For this reason, we have performed NR simulations for three different EOSs (SLy, H4, MPA1) to describe dense matter up to $n_{\rm TOV}$. Above this density, we have used five different extensions per EOS to investigate if there is an effect of the unstable branch on observable quantities during the binary NS merger. To increase the sample size of our study, we have used five different total masses, selected in such a way as to ensure that $n_{\rm TOV}$ is reached during the postmerger evolution.

During our simulations, we found no noticeable effect of the EOS in the unstable branch in any of our simulations. Indeed, the collapse time, i.e., the time between the merger and the black hole formation, only changes by a few hundred microseconds, and the emitted GW signal and the amount of ejected material seem to be independent of the particular extension used above $n_{\rm TOV}$. We point out that some of these extensions ($\Gamma = 2.50$) are extreme and become even noncausal in some parts of the simulation. Based on these observations and given current and expected future observational uncertainties, we suggest that it is unrealistic to expect that binary NS mergers will allow us to probe densities beyond those probed in high-mass pulsars. Certainly, we cannot rule out that there might be a particular combination of source parameters or a

phase transition leading to sudden density jumps that might be observable. However, given our set of simulations, the attempt to fine-tune parameters to find such a postmerger difference, and the low S/N that most binary NS observations are expected to have, it seems unlikely that binary NS mergers can be used to test densities above $n_{\rm TOV}$. Moreover, it is worth noting that EOSs for stable hybrid stars, with phase transitions below $n_{\rm TOV}$ of the hadronic branch, are not in contradiction with these findings. In this case, what matters is $n_{\rm TOV}$ that lies on the hybrid branch.

ORCID iDs

Maximiliano Ujevic ⓘ https://orcid.org/0000-0003-2869-4449
Rahul Somasundaram ⓘ https://orcid.org/0000-0003-0427-3893
Tim Dietrich ⓘ https://orcid.org/0000-0003-2374-307X
Ingo Tews ⓘ https://orcid.org/0000-0003-2656-6355

References

Abbott, B. P., Abbott, R., Abbott, T. D., et al. 2017, PhRvL, 119, 161101
Abbott, B. P., Abbott, R., Abbott, T. D., et al. 2018, PhRvL, 121, 161101
Abbott, B. P., Abbott, R., Abbott, T. D., et al. 2019, PhRvX, 9, 011001
Abbott, B., Abbott, R., Abbott, T. D., et al. 2020, ApJL, 892, L3
Alcubierre, M., Brügmann, B., Diener, P., et al. 2003, PhRvD, D67, 084023
Annala, E., Gorda, T., Kurkela, A., & Vuorinen, A. 2018, PhRvL, 120, 172703
Anton, L., Zanotti, O., Miralles, J. A., et al. 2006, ApJ, 637, 296
Antoniadis, J., Freire, P. C., Wex, N., et al. 2013, Sci, 340, 6131
Banyuls, F., Font, J. A., Ibanez, J. M. A., Marti, J. M. A., & Miralles, J. A. 1997, ApJ, 476, 221
Bauswein, A., Bastian, N.-U. F., Blaschke, D. B., et al. 2019, PhRvL, 122, 061102

Bauswein, A., Janka, H.-T., & Oechslin, R. 2010, PhRvD, D82, 084043
Bauswein, A., Just, O., Janka, H.-T., & Stergioulas, N. 2017, ApJ, 850, L34
Bernuzzi, S., & Dietrich, T. 2016, PhRv, D94, 064062
Bernuzzi, S., & Hilditch, D. 2010, PhRv, D81, 084003
Bona, C., Massó, J., Stela, J., & Seidel, E. 1996, in The Seventh Marcel Grossmann Meeting: On Recent Developments in Theoretical and Experimental General Relativity, Gravitation, and Relativistic Field Theories, ed. R. T. Jantzen, G. M. Keiser, & R. Ruffini (Singapore: World Scientific)
Branchesi, M., Maggiore, M., Alonso, D., et al. 2023, JCAP, 07, 068
Breschi, M., Gamba, R., Borhanian, S., Carullo, G., & Bernuzzi, S. 2022, arXiv:2205.09979
Bruegmann, B., Gonzalez, J. A., Hannam, M., et al. 2008, PhRvD, 77, 024027
Camelio, G., Dietrich, T., Rosswog, S., & Haskell, B. 2021, PhRvD, 103, 063014
Capano, C. D., Tews, I., Brown, S. M., et al. 2020, NatAs, 4, 625
Clark, J. A., Bauswein, A., Stergioulas, N., & Shoemaker, D. 2016, CQGra, 33, 085003
Cromartie, H. T., Fonseca, E., Ransom, S. M., et al. 2019, NatAs, 4, 72
Demorest, P., Pennucci, T., Ransom, S., Roberts, M., & Hessels, J. 2010, Natur, 467, 1081
Dietrich, T., Bernuzzi, S., Ujevic, M., & Brügmann, B. 2015a, PhRvD, D91, 124041
Dietrich, T., Coughlin, M. W., Pang, P. T. H., et al. 2020, Sci, 370, 1450
Dietrich, T., Moldenhauer, N., Johnson-McDaniel, N. K., et al. 2015b, PhRvD, D92, 124007
Dietrich, T., Radice, D., Bernuzzi, S., et al. 2018, CQGra, 35, 24LT01
Douchin, F., & Haensel, P. 2001, A&A, 380, 151
Essick, R., Tews, I., Landry, P., Reddy, S., & Holz, D. E. 2020, PhRvC, 102, 055803
Evans, M. & others (Cosmic Explorer Consortium) 2021, arXiv:2109.09882
Figura, A., Lu, J. J., Burgio, G. F., Li, Z. H., & Schulze, H. J. 2020, PhRvD, 102, 043006
Fonseca, E., Cromartie, H. T., Pennucci, T. T., et al. 2021, ApJL, 915, L12
Fryer, C. L., Fontes, C. J., Korobkin, O., et al. 2023, in 16th Marcel Grossmann Meeting on Recent Developments in Theoretical and Experimental General Relativity, Astrophysics and Relativistic Field Theories, ed. R. Ruffini & G. Vereshchagin (Singapore: World Scientific), 1391
Gaskin, J. A., Swartz, D. A., Vikhlinin, A., et al. 2019, JATIS, 5, 021001
Ghosh, S., Pradhan, B. K., Chatterjee, D., & Schaffner-Bielich, J. 2022, FrASS, 9, 864294
Gorda, T., Komoltsev, O., & Kurkela, A. 2023a, ApJ, 950, 107
Gorda, T., Kurkela, A., Paatelainen, R., Säppi, S., & Vuorinen, A. 2021, PhRvL, 127, 162003
Gorda, T., Kurkela, A., Romatschke, P., Säppi, S., & Vuorinen, A. 2018, PhRvL, 121, 202701
Gorda, T., Paatelainen, R., Säppi, S., & Seppänen, K. 2023b, PhRvL, 131, 181902
Heinzel, J., Coughlin, M. W., Dietrich, T., et al. 2021, MNRAS, 502, 3057
Hilditch, D., Bernuzzi, S., Thierfelder, M., et al. 2013, PhRvD, D88, 084057
Huth, S., Pang, P. T. H., Tews, I., et al. 2022, Natur, 606, 276
Komoltsev, O., & Kurkela, A. 2022, PhRvL, 128, 202701
Lackey, B. D., Nayyar, M., & Owen, B. J. 2006, PhRvD, 73, 024021
Landry, P., & Essick, R. 2019, PhRvD, 99, 084049
Margalit, B., & Metzger, B. D. 2017, ApJL, 850, L19
Marti, J. M., Ibanez, J. M., & Miralles, J. A. 1991, PhRvD, D43, 3794
Miller, M. C., Lamb, F. K., Dittmann, A. J., et al. 2019, ApJL, 887, L24
Miller, M. C., Lamb, F. K., Dittmann, A. J., et al. 2021, ApJL, 918, L28
Most, E. R., Papenfort, L. J., Dexheimer, V., et al. 2019, PhRvL, 122, 061101
Most, E. R., Weih, L. R., Rezzolla, L., & Schaffner-Bielich, J. 2018, PhRvL, 120, 261103
Mushotzky, R. F., Aird, J., Barger, A. J., et al. 2019, BAAS, 51, 107
Müther, H., Prakash, M., & Ainsworth, T. L. 1987, PhLB, 199, 469
Pang, P. T. H., Dietrich, T., Coughlin, M. W., et al. 2023, NatCo, 14, 8352
Punturo, M., Abernathy, M., Acernese, F., et al. 2010, CQGra, 27, 194002
Raaijmakers, G., Greif, S. K., Hebeler, K., et al. 2021, ApJL, 918, L29
Raaijmakers, G., Greif, S. K., Riley, T. E., et al. 2020, ApJL, 893, L21
Radice, D., & Dai, L. 2019, EPJA, A55, 50
Read, J. S., Lackey, B. D., Owen, B. J., & Friedman, J. L. 2009, PhRvD, D79, 124032
Reisswig, C., & Pollney, D. 2011, CQGra, 28, 195015
Reitze, D., Adhikari, R. X., Ballmer, S., et al. 2019, BAAS, 51, 035
Rezzolla, L., & Takami, K. 2016, PhRvD, D93, 124051
Riley, T. E., Watts, A. L., Bogdanov, S., et al. 2019, ApJL, 887, L21
Riley, T. E., Watts, A. L., Ray, P. S., et al. 2021, ApJL, 918, L27
Ruiz, M., Shapiro, S. L., & Tsokaros, A. 2018, PhRvD, D97, 021501
Somasundaram, R., Tews, I., & Margueron, J. 2023, PhRvC, 107, L052801
Thierfelder, M., Bernuzzi, S., & Brügmann, B. 2011a, PhRvD, D84, 044012
Thierfelder, M., Bernuzzi, S., Hilditch, D., Brügmann, B., & Rezzolla, L. 2011b, PhRvD, D83, 064022
Tichy, W. 2009, CQGra, 26, 175018
Tichy, W. 2012, PhRvD, 86, 064024
Tichy, W., Rashti, A., Dietrich, T., Dudi, R., & Brügmann, B. 2019, PhRvD, 100, 124046
van Meter, J. R., Baker, J. G., Koppitz, M., & Choi, D.-I. 2006, PhRvD, D73, 124011
York, J. W. J. 1999, PhRvL, 82, 1350
Zhang, S.-N., Santangelo, A., Feroci, M., et al. 2019, SCPMA, 62, 29502